Biomaterials 33 (2012) 2508–2520

Contents lists available at SciVerse ScienceDirect

Biomaterials

journal homepage: www.elsevier.com/locate/biomaterials

The efficiency of tumor-specific pH-responsive peptide-modified polymeric micelles containing paclitaxel

Bing-Xiang Zhao [a], Yang Zhao [a], Yue Huang [a], Lin-Min Luo [a], Ping Song [a], Xin Wang [a], Su Chen [a], Ke-Fu Yu [a], Xuan Zhang [a,*], Qiang Zhang [a,b]

[a] Department of Pharmaceutics, School of Pharmaceutical Sciences, Peking University, Xueyuan road, 38, Beijing 100191, China
[b] State Key Laboratory of Natural and Biomimetic Drugs, School of Pharmaceutical Sciences, Peking University, Beijing 100191, China

ARTICLE INFO

Article history:
Received 11 November 2011
Accepted 26 November 2011
Available online 23 December 2011

Keywords:
Tumor pH
pH-responsive peptide
Polymeric micelles
Targeting
anti-Tumor efficacy

ABSTRACT

The acidic pH in tumor tissues could be used for targeting solid tumors. In the present study, we designed a tumor-specific pH-responsive peptide $H_7K(R_2)_2$, which could respond to the acidic pH in tumor tissues, and prepared $H_7K(R_2)_2$-modified polymeric micelles containing paclitaxel (PTX-PM-$H_7K(R_2)_2$) in order to evaluate their potential targeting of tumor cells and tumor endothelial cells and their anti-tumor activity in mice with tumor cells. PTX-PM-$H_7K(R_2)_2$ was prepared by a thin-film hydration method. The *in vitro* release of PTX from PTX-PM-$H_7K(R_2)_2$ was tested. The *in vitro* targeting characteristics of $H_7K(R_2)_2$-modified polymeric micelles on HUVEC (human umbilical vein endothelial cells) and MCF-7 (human breast adenocarcinoma cells) were evaluated. The *in vivo* targeting activity of $H_7K(R_2)_2$-modified polymeric micelles and the *in vivo* anti-tumor activity of PTX-PM-$H_7K(R_2)_2$ were also investigated in MCF-7 tumor-bearing mice. The released PTX from the PTX-PM-$H_7K(R_2)_2$ was not affected by the pH. The targeting activity of the $H_7K(R_2)_2$-modified polymeric micelles was demonstrated by *in vitro* flow cytometry and confocal microscopy as well as *in vivo* biodistribution. PTX-PM-$H_7K(R_2)_2$ produced very marked anti-tumor and anti-angiogenic activity in MCF-7 tumor-bearing mice *in vivo*.

1. Introduction

Polymeric micelles are an attractive type of carrier for drug delivery system in cancer therapy [1–4]. Because of their small size (10–200 nm), they are able to extravasate through the leaky vasculature of tumor tissues upon i.v. administration due to enhanced permeation and retention (EPR) effect [5,6], which makes them highly promising as a passively targeted drug delivery system. Targeted polymeric micelles, modified with targeting ligands or antibodies to allow the drugs carried to selectively accumulate in the target tissue, have the potential to increase the therapeutic efficacy of tumor therapy [7]. However, these approaches have achieved only limited success in clinical situations because of the heterogeneous cell populations as well as differential receptor or antigen expression on tumor cell surfaces [8,9]. In addition, both the presence of antigens and the expression of receptors on the surface of these tumor cells are transient and dynamic. The heterogeneity of cancer cells may explain the reasons for some of the unexpected results obtained with this targeting strategy [10].

Unlike the complex issues associated with targeting the phenotype of tumor cells, the pH differences between the solid tumor and normal tissues (or blood) are relatively simple and intrinsic [11]. The extracellular pH (pHe) in most tumors is more acidic (pH 6.5–7.2) than that in normal tissues (pH 7.4) [12]. Therefore, smart drug carriers that respond to pH stimuli can be potentially used for tumor-specific anti-tumor drug delivery [13]. Polymeric micelles containing pH-responsive histidine and sulfonamide moieties have been designed to present a sharp pH-dependent micellization/demicellization transition, resulting in demicellization leading to rapid drug release in target tumor tissues [14,15]. However, some pH-responsive polymeric micelles in acidic pH buffer might take a few hours to exhibit this sharp pH-dependent response. Therefore, a relatively long reaction time is needed for these pH-responsive polymeric micelles to exhibit a pH response. In addition, the *in vivo* pH response of various polymeric

* Corresponding author. Tel./fax: +86 10 82802683.
E-mail address: xuanzhang@bjmu.edu.cn (X. Zhang).

0142-9612/$ – see front matter © 2011 Elsevier Ltd. All rights reserved.
doi:10.1016/j.biomaterials.2011.11.078

micelles at the target tumor tissue might be less effective than that under *in vitro* pH buffer conditions, due to the very small tumor volume and the lower tumor targeting ability.

It is well known that cell-penetrating peptides (CPPs) have the ability to cross the plasma membrane barrier of mammalian cells for the intracellular or transcellular delivery of cargoes as diverse as low molecular weight drugs, imaging agents, oligonucleotides, peptides, proteins and nano-sized carriers [16–21]. By covalent conjugation of CPPs with micelles, rapid and successful delivery of the carrier into cells has been achieved [22]. However, the primary obstacle to these CPP-modified polymeric micelles for *in vivo* targeted delivery applications is the lack of selectivity [23,24]. To overcome this, polymeric micelles with a pH-induced CPP on the micelle surface have been developed [25]. These mixed polymeric micelles consist of poly (histidine)-PEG (polyHis-PEG) and PLA-PEG-polyHis-TAT. The polyHis block in PLA-PEG-polyHis-TAT is located at the interface of the hydrophobic core of PLA and polyHis and the hydrophilic PEG shell. The interfacial polyHis causes PEG chain bending and the TAT is buried in the PEG shell, derived from the polyHis-PEG block copolymer. These micelles are stable at normal blood pH and conceal the conjugated TAT. However, as the pH is reduced in the tumor microenvironment, the degree of ionization of polyHis increases. The interfacial polyHis becomes ionized first and, at the critical degree of ionization, its hydrophobic interaction with the core phase weakens. As a result, the PEG-polyHis-TAT portion expands, pushing TAT out of the PEG shell, which has the potent ability to allow the polymeric micelles to penetrate into the cells.

In this study, to enhance the specificity of CPP for targeting tumor tissues, we designed a tumor-specific pH-responsive peptide $H_7K(R_2)_2$ (the sequence is RRK(HHHHHHH)RR, Fig. 1A). It has been reported that arginine(R)-rich peptides have the ability to cross cell membranes in a seemingly energy-independent manner. The activity of branched R-rich peptides is stronger than that of those with a linear structure. The polyHis has the ability to respond to the acidic pH in the tumor microenvironment. Therefore, we believed that this $H_7K(R_2)_2$ peptide may respond to the acidic pH in tumor tissues, as triggered by H_7 and subsequently carry the polymeric micelles carrying the chemotherapeutic drugs into tumor cells, as penetrated by $(R_2)_2$. In order to prepare $H_7K(R_2)_2$ peptide-modified polymeric micelles, $H_7K(R_2)_2$ was first conjugated with PLGA-PEG (Fig. 1B). The $H_7K(R_2)_2$-modified polymeric micelles loaded with paclitaxel (PTX) were self-assembled to form stable PTX-PM-$H_7K(R_2)_2$ (Fig. 1C). HUVEC (Human umbilical vein endothelial cells) and MCF-7 (Human breast adenocarcinoma cells) were chosen as the model for endothelial cells and tumor cells. The *in vitro* and *in vivo* targeting characteristics of $H_7K(R_2)_2$-modified polymeric micelles were investigated. Furthermore, the anti-tumor activity of PTX-PM-$H_7K(R_2)_2$ was evaluated in MCF-7 tumor-bearing nude mice *in vivo*.

2. Materials and methods

2.1. Materials and animals

N-hydroxysuccinimidyl-PEG_{6000}-$PLGA_{3000}$ (NHS-PEG-PLGA, L/G = 85/15, Mw/Mn = 1.11 as determined by GPC) and $mPEG_{5000}$-$PLGA_{3000}$ (PEG-PLGA, L/G = 85/15, Mw/Mn = 1.19 as determined by GPC) were purchased from Advanced Polymer Materials Inc. (Montreal, QC, Canada). The Ac-RRK(HHHHHHH)RR-NH_2 peptide ($H_7K(R_2)_2$) was synthesized by Beijing Scilight Biotechnology Co., Ltd. (Beijing, China). Paclitaxel (PTX) was obtained from Mei-Lian Co., Ltd. (Chongqing, China). Paclitaxel injection (Taxol) was commercially available from the local hospital of Beijing (Bristol Myers Squibb Co., Princeton, NJ, USA). Near-infrared lipophilic carbocyanine dye 1,1′-dioctadecyltetramethyl indotricarbocyanine iodide (DiR) was obtained from Biotium, Inc. (Hayward, CA, USA). Fluorescent probes, including coumarin-6 and Hoechst 33258, were purchased from Molecular Probes Inc. (Eugene, OR, USA). D-α-tocopheryl polyethylene glycol 1000 succinate (TPGS) was purchased from Sigma-Aldrich (St, Louis, MO, USA). Cell culture media, RPMI 1640 and M199, penicillin-streptomycin, fetal bovine serum, and L-glutamine, were obtained from GIBCO, Invitrogen Corp. (Carlsbad, CA, USA). All other chemicals were of analytical grade.

Human breast adenocarcinoma (MCF-7) cells were obtained from the Institute of Basic Medical Sciences, Chinese Academy of Medical Sciences (Beijing, China), and were grown in RPMI 1640 medium, supplemented with 2 mmol glutamine, 1% penicillin-streptomycin and 10% fetal bovine serum. Human umbilical vein endothelial cells (HUVEC) were isolated from umbilical cords and grown to a passage of 3–5 in 75 cm^2 flasks (Nunc, Roskilde, Denmark), and maintained in culture media as described in detail earlier [26]. All the cel1s were cultured in a humidified incubator at 37 °C in an atmosphere of 5% CO_2.

Female BALB/c nude mice were purchased from the Academy of Military Medical Sciences (Beijing, China) at 6 weeks of age (initially weighing 20–25 g). All care and handling of animals were performed in accordance with the Institutional Authority for Laboratory Animal Care of Peking University.

2.2. Synthesis of PLGA-PEG-$H_7K(R_2)_2$

The PLGA-PEG-$H_7K(R_2)_2$ was synthesized by our laboratory according to a previously reported method [27]. $H_7K(R_2)_2$ was conjugated with PLGA-PEG through the NHS group. PLGA-PEG-NHS was added and incubated with $H_7K(R_2)_2$ at a 2:1 molar ratio (PLGA-PEG-NHS:$H_7K(R_2)_2$) in DMF, and the pH was adjusted to 7.0 with N-methyl morpholine. The reaction was maintained for 24 h at room temperature under moderate stirring. The resulting reaction mixture was placed in a dialysis bag (molecular weight cut off = 3500 Da) and dialyzed against deionized water for 48 h to remove the unconjugated peptides. The final solution in the dialysis bag was lyophilized and stored at −20 °C until required.

2.3. Preparation of PTX-PM-$H_7K(R_2)_2$

The PTX-loaded $H_7K(R_2)_2$-modified polymeric micelles (PTX-PM-$H_7K(R_2)_2$) were prepared by a thin-film hydration method, as described previously [27]. Briefly, PLGA-PEG-$H_7K(R_2)_2$, PEG-PLGA and TPGS at a 5:75:20 molar ratio were dissolved in methanol, and PTX was then added in a 1:20 weight ratio (PTX: total-copolymers). Following evaporation of the solvent in an RE52 rotary evaporator (Shanghai Yarong Biochemistry Instrument Company, China) in a round-bottomed flask at 45 °C for about 40 min, a solid film was formed. This film was then flushed with nitrogen gas for 30 min and stored overnight in a desiccator to remove any traces of methanol. After addition of 5% glucose solution at 60 °C and vortexing for 2 min, a micellar solution was obtained. Finally, this solution was purified by passing it through a 0.22 μm pore size membrane filter to remove un-entrapped PTX. For the preparation of un-modified polymeric micelles containing PTX (PTX-PM), an identical procedure was conducted except that the equivalent molar PLGA-PEG-$H_7K(R_2)_2$ was replaced by PEG-PLGA.

The preparation method for polymeric micelles with fluorescent reagents, including coumarin-6-PM, coumarin-6-PM-$H_7K(R_2)_2$, DiR-PM and DiR-PM-$H_7K(R_2)_2$, was exactly the same as that for PTX-loaded polymeric micelles, except that PTX was replaced by coumarin-6 or DiR.

2.4. Characterization of polymeric micelles

The particle size and zeta potential of PTX-PM-$H_7K(R_2)_2$ were measured by photon correlation spectroscopy using a Malvern Zeta sizer 3000 HS (Malvern, UK) at 25 °C. The morphology of PTX-PM-$H_7K(R_2)_2$ was characterized by transmission electron microscopy (TEM, FEI-TECNAI, Philips, Netherlands) followed by freeze-fracture A droplet of PTX-PM-$H_7K(R_2)_2$ was sandwiched between two copper electron microscopy grids, snap-frozen by immersion in liquid ethane and then loaded into a double-replica device immersed in liquid nitrogen (−196 °C). The double-replica device was mounted on the rotary sample stage of a Balzers BAF 400 D freeze etch device (Balzers, Liechtenstein) cooled to −110 °C. Fracturing was carried out under a vacuum of 3×10^{-7} mbar. The fractured surfaces were shadowed with platinum (45°) and then immediately with carbon (90°). The replicas were then washed in chloroform, methanol, and distilled water and the dried replicas were viewed with a transmission electron microscope operated at an accelerating voltage of 80 kV.

The encapsulation efficiency was estimated from the following formula:

$$\text{Encapsulation Efficiency} = \frac{\text{Actual amount of drug loaded in polyermic micelles}}{\text{Theory amount of drug loaded in polyermic micelles}} \times 100\%$$

2.5. In vitro release of PTX from PTX-PM-$H_7K(R_2)_2$

The release of PTX from PTX-PM-$H_7K(R_2)_2$ was investigated by dialysis. Briefly, a sample of PTX-PM-$H_7K(R_2)_2$ (0.2 ml, 1 mg/ml) was mixed with 0.8 ml buffer solution, placed in a dialysis tube (MWCO 7000) and tightly sealed. Then, the dialysis tube was immersed in 200 ml release medium (PBS containing 0.1% (v/v) Tween 80) and incubated in an orbital shaker for 24 h at 37 °C. Samples (0.5 ml) were taken at predetermined time intervals from the release medium over a period of 24 h, and

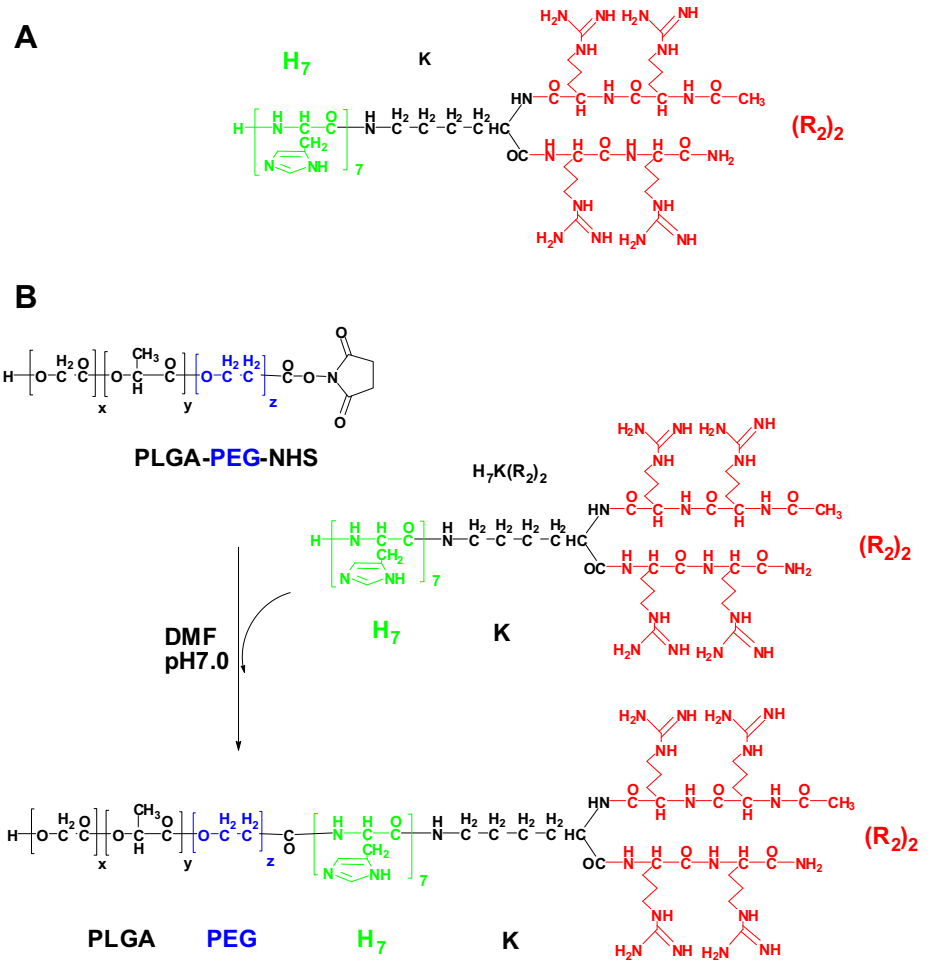
A
B
PLGA-PEG-NHS
DMF
pH7.0
PLGA
PEG
C
PLGA PEG H7 K (R2)2
PLGA PEG
Paclitaxel
TPGS
Self-assembly
PEG shell
switch off (pHb)
switch on (pHe)
Ionized His
Blood pH
Tumor pHe

Table 1
The characterization of PTX-PM-$H_7K(R_2)_2$ ($n = 3$).

Polymeric micelles		Particle size (nm)	Polydispersity	Zeta potential (mV)	Entrapment efficiency (%)
PTX-PM	pH6.8	54.37 ± 1.16	0.11 ± 0.02	−0.34 ± 0.32	
PTX-PM	pH7.4	53.02 ± 1.25	0.13 ± 0.05	−0.85 ± 0.37	97.99 ± 2.10
PTX-PM-$H_7K(R_2)_2$	pH6.8	48.21 ± 0.47	0.09 ± 0.01	0.58 ± 0.67	
PTX-PM-$H_7K(R_2)_2$	pH7.4	46.46 ± 0.37	0.10 ± 0.02	0.34 ± 0.44	96.34 ± 2.50

these were replaced by a similar volume of fresh medium. The concentration of PTX was determined by HPLC after appropriate dilution with acetonitrile and without further treatment.

2.6. Flow cytometry

HUVEC or MCF-7 cells were seeded at a density of 1×10^5 cells/well in 6-well plates and incubated at 37 °C for 24 h to allow cell attachment. After 24 h, the medium was replaced with cell culture medium (pH 6.8 or pH 7.4) containing coumarin-6 solution or coumarin-6 loaded polymeric micelles (the concentration of coumarin-6 was 100 ng/ml). After a 2 h incubation, the cells were washed three times with PBS solution. The cells were then harvested by trypsinization and centrifuged at 1000 rpm for 5 min, re-suspended in 500 μl PBS medium and examined by flow cytometry using an FACScan instrument (Becton Dickinson, San Jose, CA, USA). Cell-associated coumarin-6 was excited with an argon laser (430 nm) and fluorescence was detected at 485 nm.

2.7. Confocal microscopy studies

Following incubation of HUVEC or MCF-7 cells in glass-bottomed dishes containing culture medium at 37 °C for 24 h, cell culture media (pH 6.8 or 7.4) containing coumarin-6 solution and coumarin-6 loaded polymeric micelles were added (the final concentration of coumarin-6 was 100 ng/ml) to each dish and incubated for another 2 h at 37 °C. The medium was then removed and cells were washed with ice-cold PBS followed by fixing with 4% paraformaldehyde in PBS. After fixing, the cells were processed in a Hoechst 33258 for 15 min. The fluorescent images of the cells were analyzed using a TCS SP2 confocal microscope (Leica, Germany).

2.8. Tissue distribution of DiR-loaded polymeric micelles

Female BALB/C nude mice were inoculated subcutaneously in the right armpits with 0.1 ml MCF-7 cell suspension (4×10^6). Once the tumor masses reached approximately 200 mm^3 in volume, the mice received and intravenous injection, via the tail vein, of 5% glucose, DiR-PM or DiR-PM-$H_7K(R_2)_2$ at a dose of 50 μg/kg. The mice were then anaesthetized with intraperitoneal injection of pentobarbital (60 mg/kg), and scanned at 1, 2, 4 and 24 h using a Kodak *In Vivo* Imaging System FX PRO (Carestream Health, Inc., USA) with an excitation bandpass filter at 730 nm and an emission wavelength of 790 nm. The exposure time was 30 s per image. The fluorescent signal intensities were analyzed using Carestream MI SE software. For each NiR image, a corresponding X-ray image was taken to identify the anatomical location of the tumor. After *in vivo* imaging, the mice were sacrificed at 4 and 24 h, and the major organs, including heart, liver, spleen, lungs, kidneys, intestines, and tumors were excised. The near-infrared fluorescence signal intensities in the different tissues were measured.

2.9. In vivo anti-tumor activity

Female BALB/C nude mice were inoculated subcutaneously in the right armpits with 0.1 ml of an MCF-7 cell suspension (4×10^6). Once the tumor volume reached about 150–200 mm^3 on 5th day, the mice were randomly assigned to four groups (six animals per group): group 1 given a 5% glucose solution, group 2 given Taxol injection (15 mg/kg, i.v., q3d × 4), group 3 given PTX-PM (15 mg/kg, i.v., q3d × 4), and group 4 given PTX-PM-$H_7K(R_2)_2$ (15 mg/kg, i.v., q3d×4). For all administrations, the formulations were given via the tail vein. The total dose of PTX in all treatment groups was 60 mg/kg. Throughout the study, mice were weighed and tumors were measured with calipers every two days. Tumor volumes were calculated from the formula: V = length(cm) × width(cm^2) × 0.5236. Once animals in any group seemed moribund, all animals in the experiment were sacrificed, and the tumors were harvested and weighed.

2.10. Assay of in vivo angiogenesis

CD31 staining was used to identify the microvessel vessel density in the tumor tissues by immunohistochemistry. Briefly, after removing the paraffin from paraffin-embedded tissue sections (5 μm thick) using xylene and rehydrating in alcohol, sections were incubated in 0.3% H_2O_2 to block endogeneous peroxidase activity. Each slide was incubated with normal goat serum (Santa Cruz Biotechnology. INC, USA) for 20 min at room temperature, and then incubated in the primary antibody at 4 °C overnight. After incubation with the secondary antibody (ZSGB-BIO, China), and biotinylation for 30 min at 37 °C, each slide was rinsed in PBS and incubated in avidin-biotin peroxidase complex for 30 min at 37 °C. The peroxidase was visualized with 3-3′-diamino-benzidinetetrahydrochloride (DAB) solution followed by counterstaining with hematoxylin. MVD was assessed as described in the international consensus report (Ref?). Immuno-stained slides were scanned at ×100 magnification to identify the areas with the highest number of vessels (so called 'hot spot'). Counts were performed on 10 fields in each hot spot by two independent pathologists at × 200 magnification.

2.11. HPLC analysis of PTX

The concentration of PTX in PTX-PM-$H_7K(R_2)_2$ was determined by HPLC using a Waters HPLC system consisting of a 1525-pump, and a 2487-ultraviolet detector (Waters Co. Inc., Westerville, OH, USA) [28]. The mobile phase consisted of methanol-water-tetrahydrofuran (67.5:30:2.5, v/v/v), delivered at a flow rate of 1 ml/min. Chromatographic separation was performed on a Phenomenex ODS_3 column (250 × 4.6 mm, 5 μm, Torrance, CA, USA) and the detector wavelength was 230 nm.

2.12. Statistical analysis

All data are presented as the mean ± standard deviation (SD). One-way analysis of variance (ANOVA) was used to determine significance among groups, after which post-hoc tests with the Bonferroni correction were used for comparison between individual groups. Statistical significance was established at $p < 0.05$.

3. Results

3.1. Preparation of PTX-PM-$H_7K(R_2)_2$

As shown in Fig. 1B, $H_7K(R_2)_2$ was conjugated to the terminal of PEG through a reaction between the NHS group of PEG and the terminal amino group of the $H_7K(R_2)_2$ peptides. The results of MALDI-TOF-MS indicated that $H_7K(R_2)_2$ peptides were successfully conjugated with PLGA-PEG-NHS via an amide bond (data not shown).

In aqueous solution, PLGA-PEG (the critical micelle concentration of PLGA-PEG at pH 7.4 was 21 μg/ml) would self-assemble into polymeric micelles composed of a hydrophilic outer shell exposed to the aqueous phase and a hydrophobic inner core encapsulating the drug molecules. The detailed scheme for preparation of PTX-PM-$H_7K(R_2)_2$ is illustrated in Fig. 1C.

Fig. 1. Preparation of PTX-PM-$H_7K(R_2)_2$. A. The sequence of $H_7K(R_2)_2$ peptide; B. The schematic representation of synthesis of PLGA-PEG-$H_7K(R_2)_2$ copolymer; C. The schematic representation depicting the central concept of pH-sensitive micelles based on PLGA-PEG-$H_7K(R_2)_2$ copolymer. Oligohistidine (H_7) has the pH-dependent amphoteric properties (hydrophilic-hydrophobic) by protonation-deprotonation of the imidazole ring. During circulation in normal tissue microvasculature (pH 7.4), the cell-penetrating oligoarginine $(R_2)_2$ is anchored on the micelle core and shielded by PEG shell of the micelle due to the deionization of H_7 ($pH > pK_b$); but in tumor microenvironment (pH 6.8), R4 is exposed to the outside of PEG shell thanks to the ionization of H_7 ($pH < pK_b$), followed by interaction with tumor cells and endocytosis.

3.2. Characterization of PTX-PM-$H_7K(R_2)_2$

The particle size of PTX-PM-$H_7K(R_2)_2$ was approximately 46 ± 0.4 nm and the polydispersity was 0.10 ± 0.02. The value of the zeta potential of PTX-PM-$H_7K(R_2)_2$ was slightly positive (0.34 ± 0.44 mV). The entrapment efficiency of PTX-PM-$H_7K(R_2)_2$ was 96.34 ± 2.50% ($n = 3$), as shown in Table 1.

A typical particle size and distribution of PTX-PM-$H_7K(R_2)_2$ is shown in Fig. 2A. TEM was used to examine the morphology of PTX-PM-$H_7K(R_2)_2$, as shown in Fig. 2B. The TEM images showed that PTX-PM-$H_7K(R_2)_2$ had a spherical shape and uniform size.

3.3. In vitro release of PTX from PTX-PM-$H_7K(R_2)_2$

The results of the *in vitro* release of PTX from PTX-PM-$H_7K(R_2)_2$ in medium with a pH of 6.4, 6.8 and 7.4 are shown in Fig. 3. For PTX-PM-$H_7K(R_2)_2$ groups, the release of PTX in pH 6.4 buffer solution was slightly faster than that in pH 6.8 or 7.4 buffer, but there was no significant difference at most of the time points (Fig. 3A). However, for PTX-PM groups, the release of PTX in buffer at pH 6.4, 6.8 and 7.4 was almost identical (Fig. 3B). In addition, the release of PTX from PTX-PM-$H_7K(R_2)_2$ was also slightly faster than that from PTX-PM in pH 6.4 buffer (Fig. 3C). In buffer at pH 6.8 and 7.4, similar release patterns of PTX were observed for PTX-PM-$H_7K(R_2)_2$ and PTX-PM groups (Fig. 3D and E).

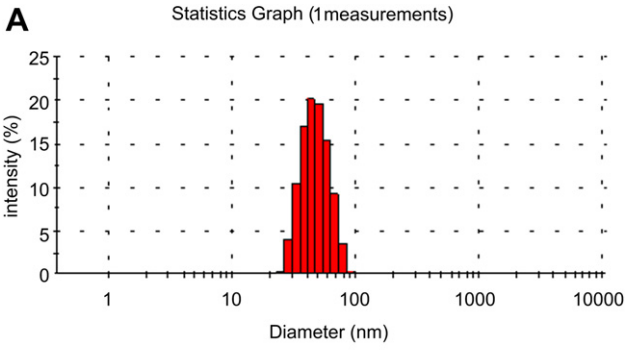

Fig. 2. A. Typical particle size and distribution of the PTX-PM-$H_7K(R_2)_2$; B. Transmission electron micrograph of PTX-PM-$H_7K(R_2)_2$ (Bar = 100 nm).

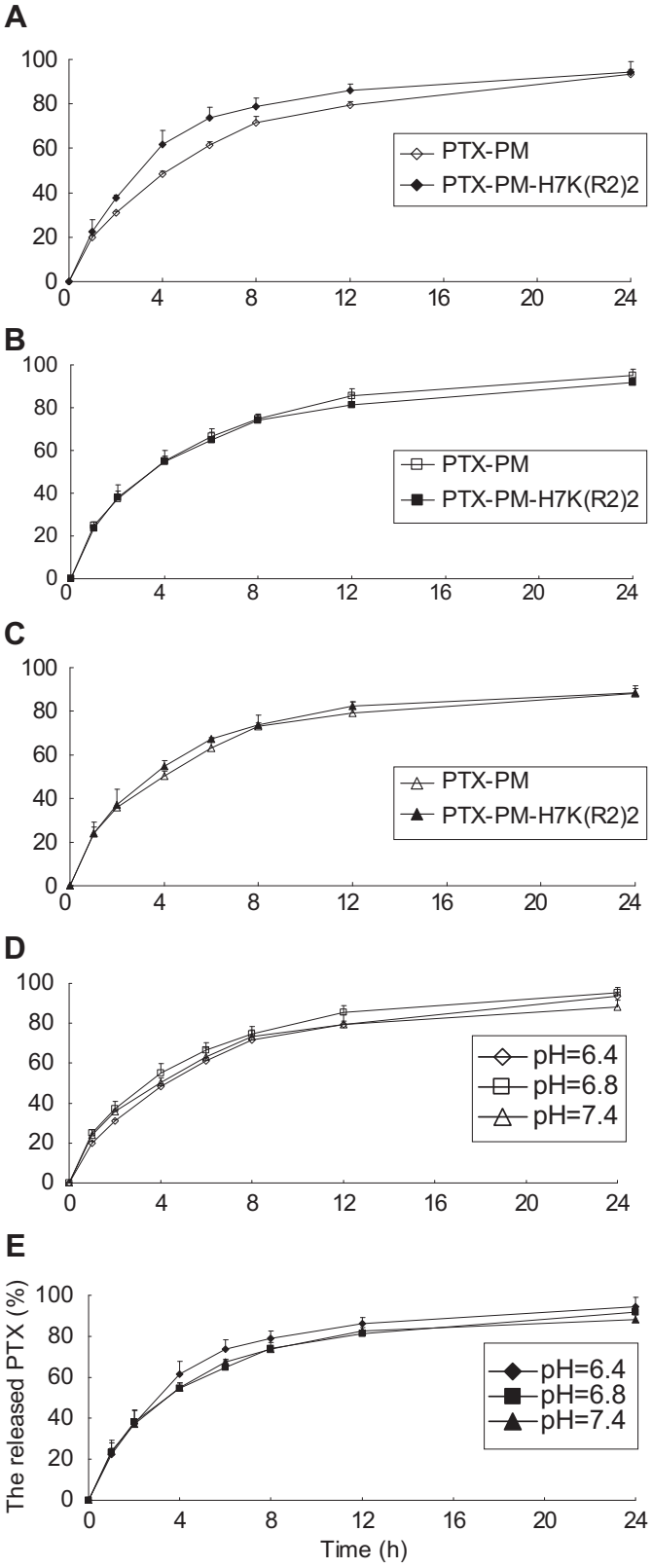

Fig. 3. The release of PTX from PTX-PM or PTX-PM-$H_7K(R_2)_2$ at 37 °C. The release medium was PBS containing 0.1% (v/v) of Tween 80. Each data represents the mean ± standard deviation ($n = 3$). A. PBS pH 6.4; B. PBS pH 6.8; C. PBS pH 7.4; D. PTX-PM; E. PTX-PM-$H_7K(R_2)_2$.

3.4. Flow cytometry analysis

Flow cytometry was used to quantify the total coumarin-6 uptake by MCF-7 or HUVEC cells for coumarin-6 formulations. As shown in Fig. 4, the cellular coumarin-6 level for coumarin-6-PM-$H_7K(R_2)_2$ in MCF-7 and HUVEC cell lines was about 1.6- and 1.3-fold higher than that for coumarin-6-PM at pH 6.8 (Fig. 4A and C). However, at pH 7.4, the intense fluorescence of coumarin-6 for coumarin-6-PM-$H_7K(R_2)_2$ and coumarin-6-PM in MCF-7 and HUVEC cell lines was almost identical (Fig. 4B and D).

3.5. Confocal microscopy studies

Fig. 5 shows the confocal microscopic images of MCF-7 and HUVEC cell lines after a 2 h incubation with coumarin-6 formulations at pH 7.4 and pH 6.8. Because of its highly hydrophobic nature, free coumarin-6 readily partitioned into the lipid membranes and then diffused into the three types of cells leading to a greater cellular accumulation, which was taken as the positive control group. For coumarin-6-PM-$H_7K(R_2)_2$, the images showed a more intense fluorescence of coumarin-6 in both MCF-7 and HUVEC cells at pH 6.8 (Fig. 5A and G) compared with pH 7.4 (Fig. 5B and H). However, for coumarin-6-PM groups, the intensity of the fluorescence of coumarin-6 at pH 6.8 was similar to that at pH 7.4 in both MCF-7 and HUVEC cells. In addition, the intense fluorescence of coumarin-6 in the coumarin-6-PM-$H_7K(R_2)_2$ group in both MCF-7 and HUVEC cells at pH 6.8 (Fig. 5A and G) was more marked than that of the coumarin-6-PM group in both MCF-7 and HUVEC cells at pH 6.8 (Fig. 5C and I). When both HUVEC and MCF-7 cells were incubated with coumarin-6 formulations at pH 7.4, the intense fluorescence of coumarin-6 in coumarin-6-PM-$H_7K(R_2)_2$ and coumarin-6-PM groups was similar.

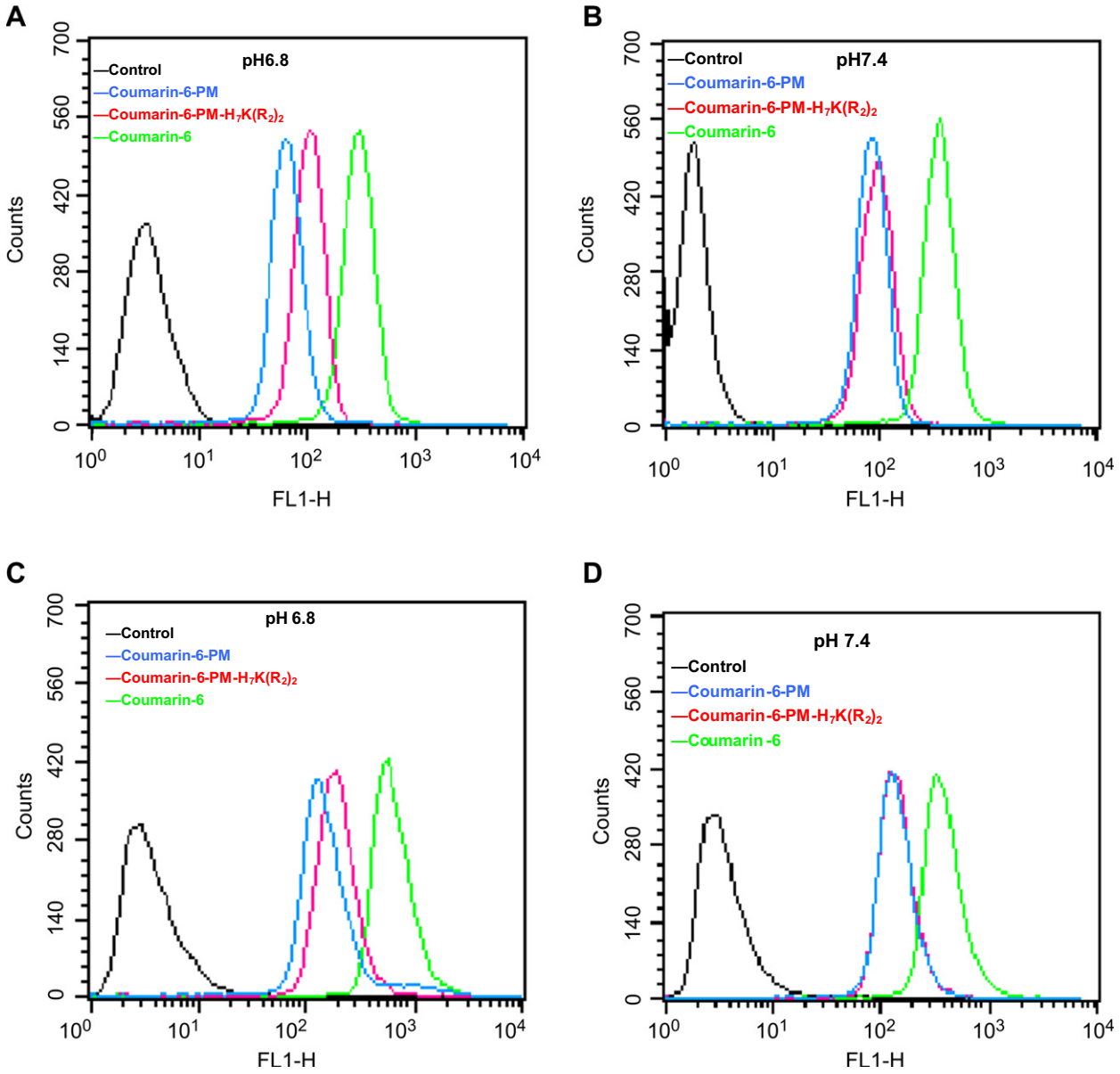

Fig. 4. Flow cytometric measurement of coumarin-6 uptake from Coumarin-6-PM or coumarin-6-PM-$H_7K(R_2)_2$ by MCF-7 cells (A, B) and HUVEC (C, D) at pH 6.8 or 7.4 (A and C at pH 6.8; B and D at pH 7.4), after incubation for 2 h at 37 °C. The final concentration of coumarin-6 was 100 ng/ml for all formulations.

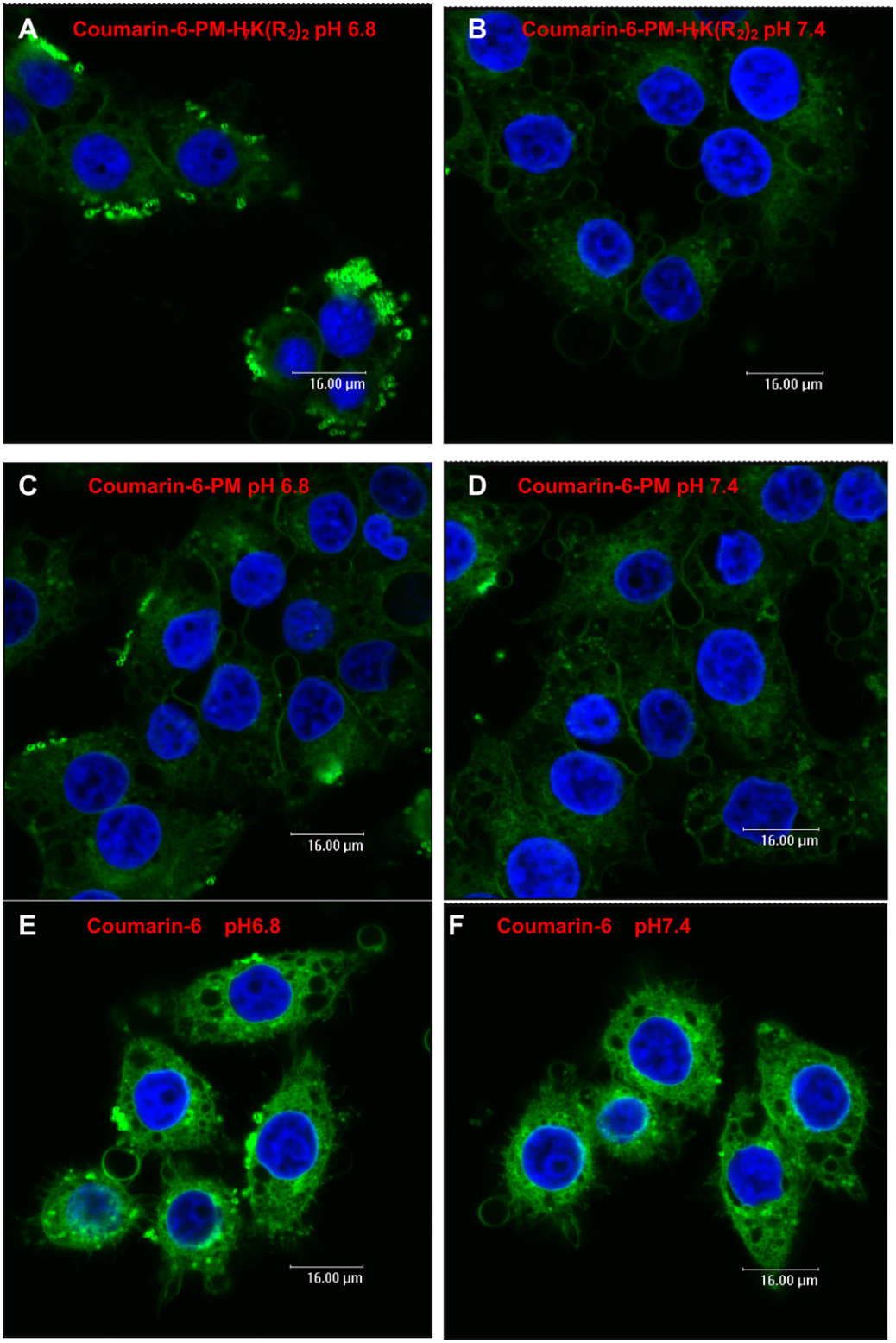

Fig. 5. Confocal microscopy images of MCF-7 cells (A–F) and HUVEC (G–L) incubated with (A, G) coumarin-6-PM-$H_7K(R_2)_2$ at pH 6.8, (B, H) coumarin-6-PM-$H_7K(R_2)_2$ at pH 7.4, (C, I) coumarin-6-PM at pH 6.8, (D, J) coumarin-6-PM at pH 7.4, (E, K) free coumarin-6 at pH 6.8, and (F, L) free coumarin-6 at pH 7.4, for 2 h at 37 °C. The final concentration of coumarin-6 was 100 ng/ml for all formulations. Green represents fluorescence of coumarin-6. Blue represents fluorescence of Hoechst 33258. (For interpretation of the references to colour in this figure legend, the reader is referred to the web version of this article.)

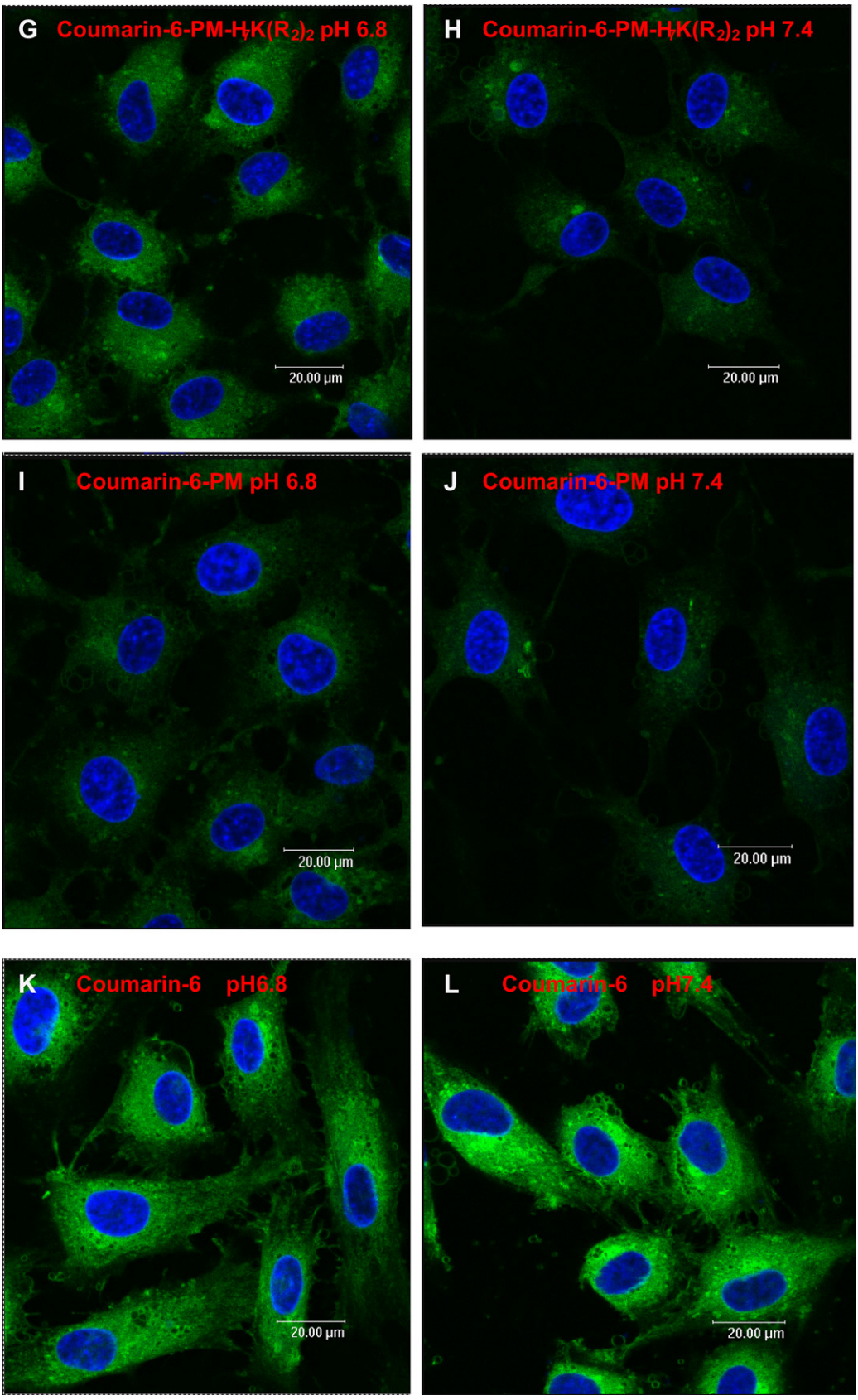

Fig. 5. (*continued*).

3.6. Tissue distribution of DiR-loaded polymeric micelles in tumor-bearing mice

Fig. 6 shows the distribution and tumor accumulation of fluorescent DiR in MCF-7 tumor-bearing mice. The DiR fluorescence signal of the tumor site was stronger for the mice treated with DiR-PM-$H_7K(R_2)_2$ than those treated with DiR-PM at all observed time points (Fig. 6A). The major organs (heart, liver, spleen, lung, kidney, intestines) and tumor tissues were isolated and the *ex vivo* images were studied. The results showed that a more intense fluorescence was found in tumor tissue after administration of DiR-PM-$H_7K(R_2)_2$ compared with administration of DiR-PM (Fig. 6B).

3.7. In vivo antitumor activity

The anti-tumor effect of PTX formulations was evaluated in MCF-7 tumor-bearing mice after cell implantation. As shown in Fig. 7, the tumor growth was significantly inhibited in all treatment groups compared with the control group given a 5% glucose injection ($p < 0.01$), but the effect obtained varied. PTX-PM-$H_7K(R_2)_2$ significantly inhibited the growth of MCF-7 tumors compared with that in the PTX-PM and Taxol treatment groups ($p < 0.01$). In addition, there was no significant difference in the anti-tumor activity between the PTX-PM group and the Taxol group ($p > 0.05$). The mean tumor size at day 21 after implantation in the PTX-PM, Taxol and PTX-PM-$H_7K(R_2)_2$ group was

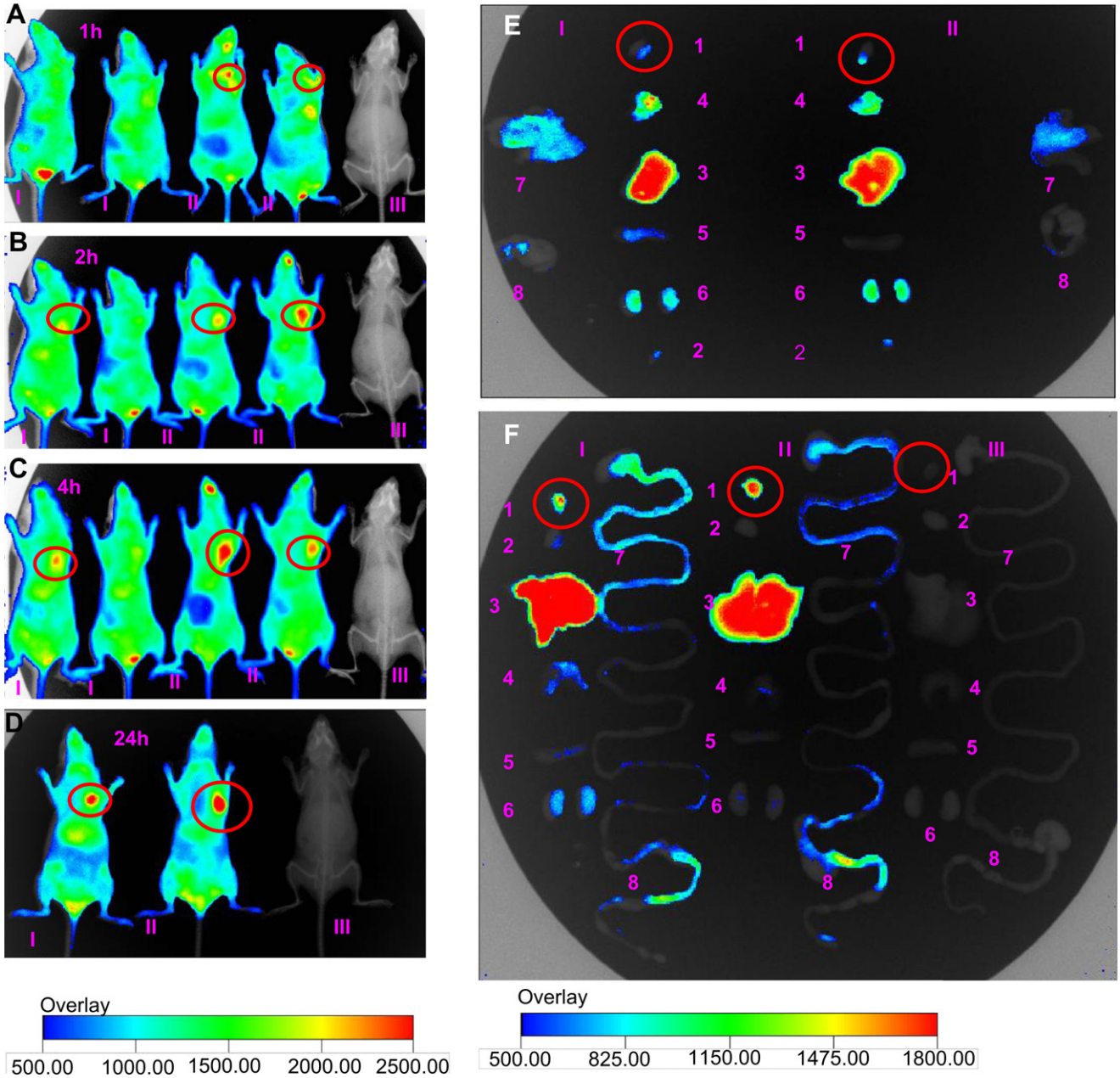

Fig. 6. *In vivo* imaging of DiR-PM-$H_7K(R_2)_2$ in tumor-bearing mice. A–D. *In vivo* whole body imaging of MCF-7 tumor-bearing mice after DiR-PM (I), DiR-PM-$H_7K(R_2)_2$ (II) and 5% glucose solution (III) administration at 1 h (A), 2 h (B), 4 h (C) and 24 h (D) time point. The *ex vivo* optical images of tumors and organs of MCF-7 tumor-bearing mice sacrificed at 4 h (E) and 24 h (F) after DiR-PM (I), DiR-PM-$H_7K(R_2)_2$ (II) and 5% glucose solution (III) administration. (1) tumors, (2) heart, (3) liver, (4) lungs, (5) spleen, (6) kidneys, (7) small intestines, (8) large intestines. Red circle represents tumor tissue. (For interpretation of the references to colour in this figure legend, the reader is referred to the web version of this article.)

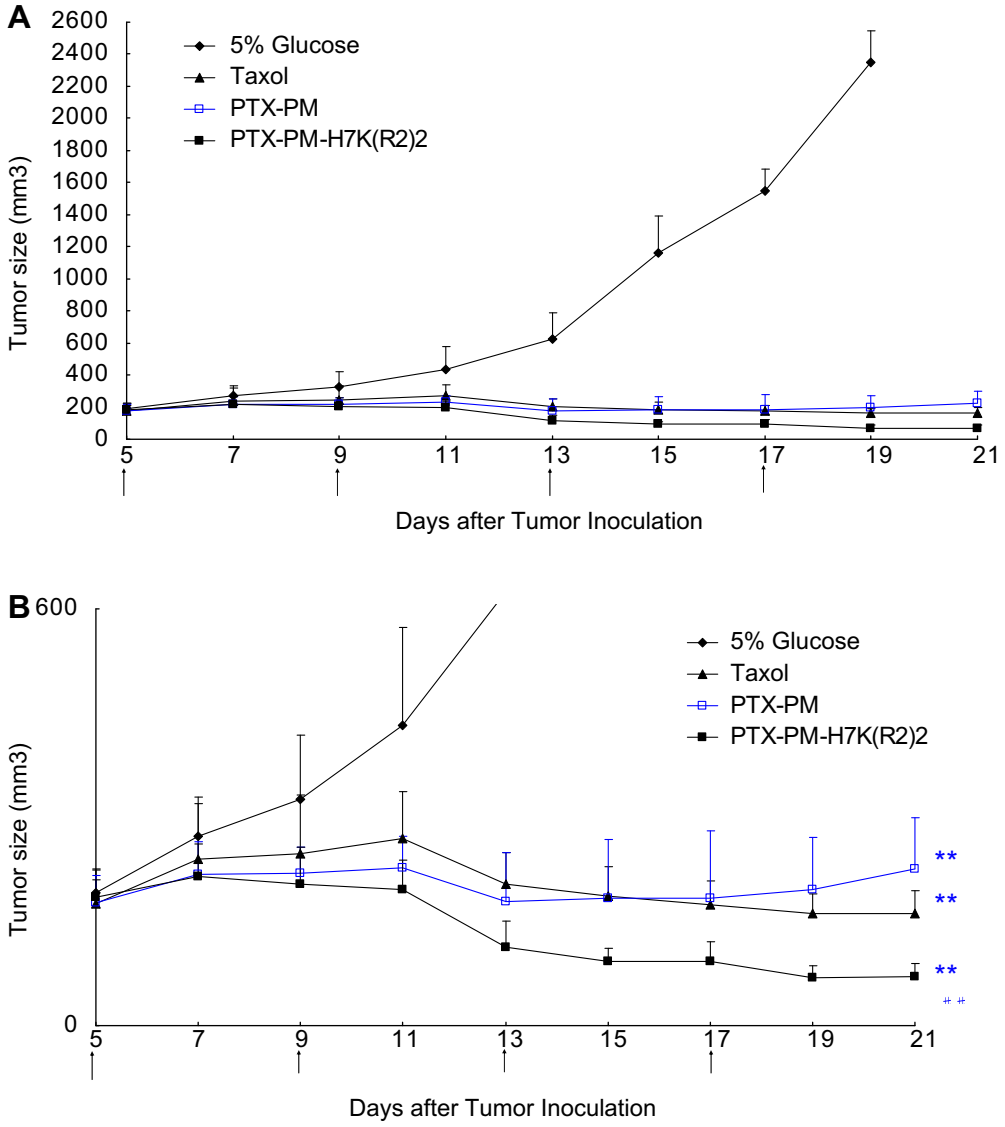

Fig. 7. Tumor growth inhibition by PTX-PM-$H_7K(R_2)_2$. BALB/C mice were inoculated s.c. with MCF-7 cells and treated with 5% glucose, Taxol, PTX-PM or PTX-PM-$H_7K(R_2)_2$ at the day 5 (15 mg/kg, i.v., q4d4, every 4 days for four doses), respectively. Tumor size was measured with calipers twice per week. Results are given as means ± S.D. ($n = 5$). A is the intact figure and B is the amplificatory figure. $^{**}p < 0.01$ vs 5% glucose injection group at the day 19; $\#\#p < 0.01$ vs Taxol or PTX-PM groups at the day 21.

226 ± 73, 161 ± 33 and 70 ± 18 mm^3, respectively, compared with 2345 ± 199 mm^3 in the control group ($p < 0.01$). The corresponding tumor growth inhibition in the PTX-PM, Taxol and PTX-PM-$H_7K(R_2)_2$ treated groups was 90.4%, 93.1% and 97.0%, respectively.

3.8. *In vivo* angiogenesis

To evaluate the anti-angiogenic activity of PTX-PM-$H_7K(R_2)_2$ treatment *in vivo*, the microvessel density was assessed by immunohistochemistry. As shown in Fig. 8A, microvessels were clearly observed by CD31 staining. Very few microvessels were observed in the PTX-PM-$H_7K(R_2)_2$ treatment group. The MVD in the PTX treatment groups was significantly less than that in the control group ($p < 0.01$), as shown in Fig. 8B. There was significantly less MVD in the PTX-PM-$H_7K(R_2)_2$ group (8.8 ± 0.4) compared with the PTX-PM (11.8 ± 0.5) and Taxol treatment groups (12.2 ± 0.8) ($p < 0.01$). Although the PTX-PM treatment was slightly higher effective than the Taxol treatment in inhibiting MVD, the difference failed to reach statistical significance.

4. Discussion

As shown in Fig. 1A, the intact peptide $H_7K(R_2)_2$ contains two functional domains: one is the CPP sequence, $(R_2)_2$, and the other is the pH trigger sequence, H_7. A lysine (K) acts as a linker to connect the H_7 and $(R_2)_2$. It has been reported that not only linear but also branched-chain arginine-rich peptides exhibit efficient internalization [29]. A four-branched chain arginine $(R_1)_4$ could enter cells to some extent. Therefore, the two-branched chain arginine $(R_2)_2$ in our $H_7K(R_2)_2$ peptide was designed as a CPP functional domain. Due to the lone pair of electrons on the unsaturated nitrogen in the imidazole ring of histidine, polyhistidine (polyHis) is pH-dependently amphoteric by protonation-deprotonation of the imidazole ring [30–34]. The ionization of polyHis switches it from hydrophobic to hydrophilic [30,31]. Therefore, we would suggest that the H_7 in our $H_7K(R_2)_2$ peptide

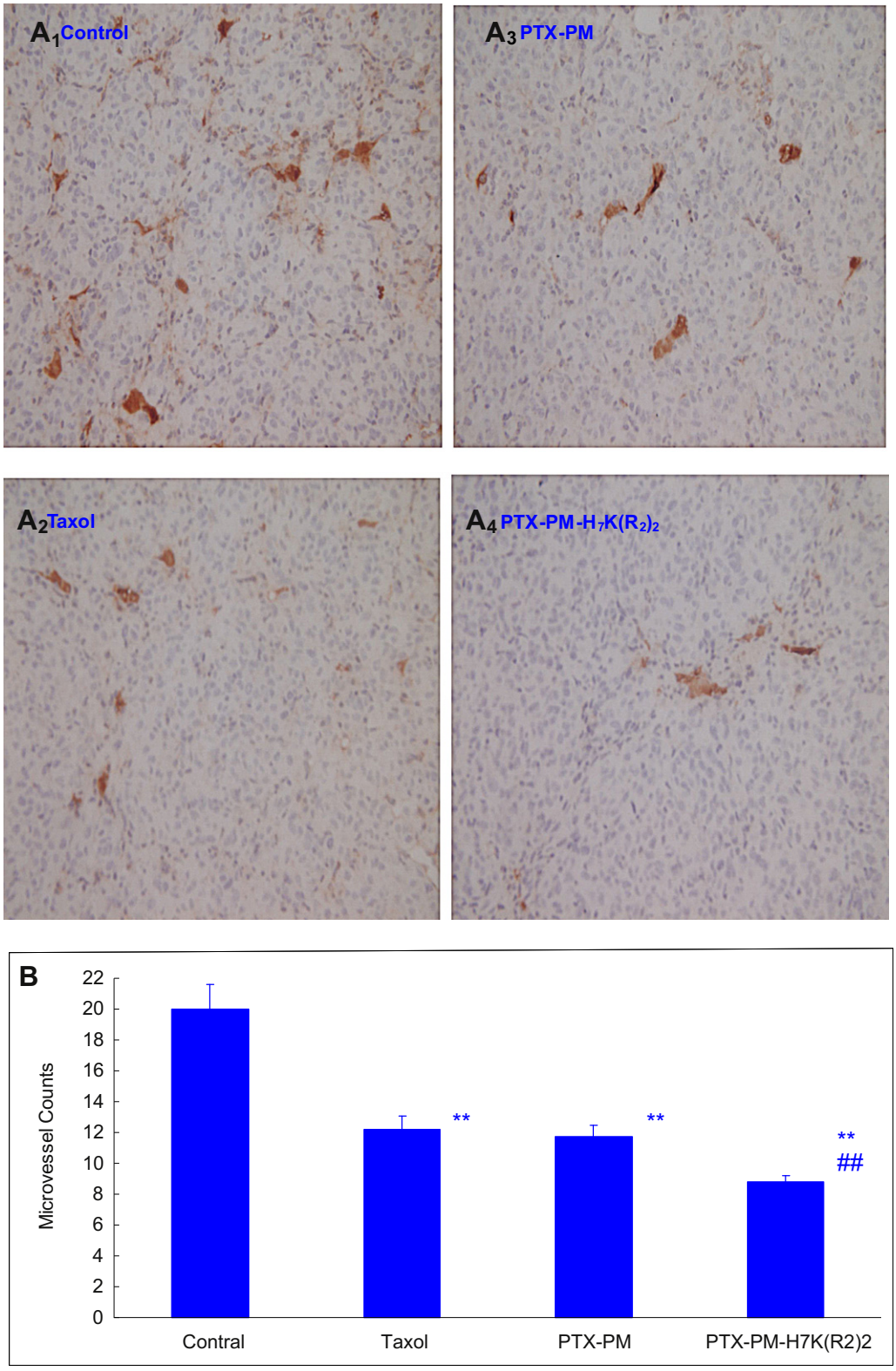

Fig. 8. Effect of PTX-PM-H7K(R2)2 on microvessel density (MVD) in xenograft MCF-7 tumors.A: Representative micrographs of immunohistochemical detection of CD31-positive microvessel in xenograft MCF-7 tumors from different treatment groups. A1: 5% glucose injection as control; A2: Taxol; A3: PTX-PM; A4: PTX-PM-H7K(R2)2; B: Mean CD31-positive microvessel counts in xenograft MCF-7 tumors in control group, treatment groups of Taxol, PTX-PM or PTX-PM-H7K(R2)2. Data are presented as the means ± SD ($n = 5$). **, $p < 0.01$, vs control treatment group; $^{\#\#}p < 0.01$, vs Taxol or PTX-PM treatment group.

would respond to the acidic pH in tumor tissue and switch from hydrophobic to hydrophilic. More importantly, unlike polyHis-TAT, this $H_7K(R_2)_2$ peptide was synthesized using a Fmoc solid-phase method to obtain an intact peptide sequence [35]. This simple synthetic method could closely control the chain length and molecule weight of the polyHis.

The model of PTX-PM-$H_7K(R_2)_2$ and the influence of pH on the micellar structure are shown in Fig. 1C. The acidic pH in tumor

tissues was used as a trigger for $(R_2)_2$ exposure on the polymeric micelle surface. During blood circulation (pH 7.4), the H_7 moiety in PLGA-PEG-$H_7K(R_2)_2$ is located at the interface of the hydrophobic PLGA core and the $(R_2)_2$ is located in the hydrophilic PEG shell. However, as the pH is lowered in the tumor pHe (in tumoral environments), the degree of protonation of the imidazole ring of H_7 increased. The interfacial H_7 became ionized and, at a critical degree of ionization, its hydrophobic interaction with the core phase weakened. This protonation of the imidazole ring would change the nature of H_7 from hydrophobic to hydrophilic. As a result, the $H_7K(R_2)_2$ portion expanded, exposing $(R_2)_2$ from the PEG shell as shown in Fig. 1C. The exposed $(R_2)_2$ could interact with tumor cells and allow the polymeric micelles to penetrate into the tumor cells.

The pH-triggered penetration of the $H_7K(R_2)_2$-modified micelles was shown by our *in vitro* results obtained from flow cytometry (Fig. 4) and confocal microscopy (Fig. 5) studies. The level of coumarin-6 in MCF-7 cells after incubation with $H_7K(R_2)_2$-modified polymeric micelles was significant higher than that after incubation with un-modified polymeric micelles in pH 6.8 medium (Figs. 4A and 5A), while the cellular coumarin-6 levels for both $H_7K(R_2)_2$-modified polymeric micelles and un-modified polymeric micelles were almost identical at pH 7.4 (Figs. 4B and 5B). It has been reported that the change in pH from 7.4 to 6.0 may affect the cell surface charge, cellular physiology and viability [11]. Therefore, in our *in vitro* experiments, the pH for cell incubation was set at 6.8. We would suggest that the penetration of the $H_7K(R_2)_2$-modified micelles would be enhanced under more acidic pH conditions. Our *in vivo* biodistribution results also showed the specific distribution of the $H_7K(R_2)_2$-modified polymeric micelles in tumor tissue (Fig. 6).

A common approach for targeted drug delivery is to functionalize the surface of the delivery systems with targeting ligands that specifically bind to the receptors overexpressed by the target cells. However, the limitation of this strategy has been pointed out by many researchers. The acidic pH in the tumor tissues is due to a tumor phenotype caused by anaerobic respiration and subsequent glycolysis [36]. In addition, the tumor pHe (but not normal tissues) may be lowered by 0.2–0.4 pH units by glucose given orally or intravenously [37,38]. Here, we report an alternative approach to targeted drug delivery. Instead of using targeting ligands to actively direct the drug carriers to the tumor cell, we have taken advantage of the acidic pH in tumor tissue to allow the $H_7K(R_2)_2$ peptide carrying the polymeric micelles to penetrate into tumor cells to exhibit their targeting action. The anti-tumor activity of PTX-PM-$H_7K(R_2)_2$ has been observed in our *in vivo* experiment (Fig. 7). PTX-PM-$H_7K(R_2)_2$ significantly inhibited the growth of MCF-7 tumors compared with that in the PTX-PM and Taxol treatment groups ($p < 0.01$). There was no significant difference in the anti-tumor activity between the PTX-PM group and the Taxol group ($p > 0.05$). In addition, the anti-tumor activity of PTX-PM-$H_7K(R_2)_2$ in HT1080 tumor-bearing mice also agrees with our *in vivo* experiments (data not shown). Therefore, we would suggest that this weakly acidic pH could be used for targeting most solid tumors, but not for specific tumor receptor targeting.

Angiogenesis is an important factor in the progression and enlargement of solid neoplasms and has a close relationship with invasion and metastases [39–42]. The proliferation of endothelial cells plays a key role in tumor angiogenesis. For this reason, many studies have focused on antiangiogesis or target endothelial cell receptors, such as using cationic liposomes as a carrier specifically binding to the endothelial cell surface [43,44]. It has been reported that endothelial cells forming the branched vasculature supporting solid tumors express an increased amount of phosphatidylserine molecules on the outer leaflet of their plasma membrane [45,46]. The histidine-rich peptides would specifically bind to these phosphatidylserine molecules to exert a direct action on the sensitive new capillary tubes. In addition, the pH at the venous end of the capillaries in tumor tissue is about 6.5 [47]. Therefore, the penetrating activity of the $H_7K(R_2)_2$-modified polymeric micelles was also investigated in HUVEC cells at an acidic pH *in vitro*, showing similar results of MCF-7 cells (Fig. 4C, D and Fig. 5G, H). The anti-angiogenic activity of PTX-PM-$H_7K(R_2)_2$ was also evaluated and confirmed in our *in vivo* studies (Fig. 8).

It is well-known that pH-sensitive polymeric micelles are attractive because of their structural destabilization at an acidic pH, resulting in rapid drug release [25,31,32,48–51]. Unlike these pH-sensitive polymeric micelles, our *in vitro* release results showed that PTX released from PTX-PM-$H_7K(R_2)_2$ was almost unaffected by the pH (Fig. 3), indicating that the $H_7K(R_2)_2$ on the micelle surface does not destabilize the micelle core structure at an acidic pH. In addition, the particle size and distribution of PTX-PM-$H_7K(R_2)_2$ was also unaffected by the pH, as shown in Table 1. Therefore, we would suggest that when pH-sensitive material is incorporated in micelles, a rapid drug release would be obtained under acidic pH conditions.

5. Conclusions

In summary, we designed a $H_7K(R_2)_2$ with pH-triggered cell penetration activity and conjugated this peptide with PLGA-PEG. The $H_7K(R_2)_2$-modified polymeric micelles containing PTX was prepared and characterized. Unlike normal pH-responsive polymeric micelles, the release of PTX from PTX-PM-$H_7K(R_2)_2$ was no affected by the pH. The specific targeting effect of $H_7K(R_2)_2$-modified polymeric micelles triggered by acidic pH was observed in our *in vitro* experiments in MCF-7 and HUVCE cells and *in vivo* experiments in MCF-7 tumor-bearing mice. The anti-tumor and anti-angiogenic activity of PTX-PM-$H_7K(R_2)_2$ has been found in our *in vivo* experiments. This $H_7K(R_2)_2$-modified polymeric micelles containing anti-tumor drugs developed in this study are a promising delivery system for anti-tumor therapy for response stimuli of the acidic pH in tumor microenvironment.

Acknowledgements

The authors gratefully acknowledge the financial support from the National natural science foundation of China (National natural science foundation of China) (No. 30873170) and the National Basic Research Program of China (National Basic Research Program of China) (973 Program 2007CB935800 and 2009CB930300).

References

[1] Oerlemans C, Bult W, Bos M, Storm G, Nijsen JF, Hennink WE. Polymeric micelles in anticancer therapy: targeting, imaging and triggered release. Pharm Res 2010;27(12):2569–89.
[2] Kataoka K, Harada A, Nagasaki Y. Block copolymer micelles for drug delivery: design, characterization and biological significance. Adv Drug Deliv Rev 2001; 47(1):113–31.
[3] Adams ML, Lavasanifar A, Kwon GS. Amphiphilic block copolymers for drug delivery. J Pharm Sci 2003;92(7):1343–55.
[4] Lavasanifar A, Samuel J, Kwon GS. Poly(ethylene oxide)-block-poly(L-amino acid) micelles for drug delivery. Adv Drug Deliv Rev 2002;54(2):169–90.
[5] Talelli M, Iman M, Varkouhi AK, Rijcken CJ, Schiffelers RM, Etrych T, et al. Core-crosslinked polymeric micelles with controlled release of covalently entrapped doxorubicin. Biomaterials 2010;31(30):7797–804.
[6] Greish K. Enhanced permeability and retention of macromolecular drugs in solid tumors: a royal gate for targeted anticancer nanomedicines. J Drug Target 2007;15(7–8):457–64.
[7] Bae Y, Kataoka K. Intelligent polymeric micelles from functional poly(ethylene glycol)-poly(amino acid) block copolymers. Adv Drug Deliv Rev 2009;61(10): 768–84.

[8] Duncan R. Polymer conjugates as anticancer nanomedicines. Nat Rev Cancer 2006;6(9):688–701.
[9] Parker N, Turk MJ, Westrick E, Lewis JD, Low PS, Leamon CP. Folate receptor expression in carcinomas and normal tissues determined by a quantitative radioligand binding assay. Anal Biochem 2005;338(2):284–93.
[10] Lee ES, Gao Z, Bae YH. Recent progress in tumor pH targeting nanotechnology. J Control Release 2008;132(3):164–70.
[11] Tannock IF, Rotin D. Acid pH in tumors and its potential for therapeutic exploitation. Cancer Res 1989;49(16):4373–84.
[12] Engin K, Leeper DB, Cater JR, Thistlethwaite AJ, Tupchong L, McFarlane JD. Extracellular pH distribution in human tumours. Int J Hyperthermia 1995; 11(2):211–6.
[13] Felber AE, Dufresne MH, Leroux JC. pH-sensitive vesicles, polymeric micelles, and nanospheres prepared with polycarboxylates. Adv Drug Deliv Rev; 2011. PMID: 21996056.
[14] Sethuraman VA, Bae YH. TAT peptide-based micelle system for potential active targeting of anti-cancer agents to acidic solid tumors. J Control Release 2007;118(2):216–24.
[15] Sethuraman VA, Lee MC, Bae YH. A biodegradable pH-sensitive micelle system for targeting acidic solid tumors. Pharm Res 2008;25(3):657–66.
[16] Foged C, Nielsen HM. Cell-penetrating peptides for drug delivery across membrane barriers. Expert Opin Drug Deliv 2008;5(1):105–17.
[17] Rousselle C, Clair P, Lefauconnier JM, Kaczorek M, Scherrmann JM, Temsamani J. New advances in the transport of doxorubicin through the blood-brain barrier by a peptide vector-mediated strategy. Mol Pharmacol 2000;57(4):679–86.
[18] Ruan G, Agrawal A, Marcus AI, Nie S. Imaging and tracking of tat peptide-conjugated quantum dots in living cells: new insights into nanoparticle uptake, intracellular transport, and vesicle shedding. J Am Chem Soc 2007; 129(47):14759–66.
[19] Said Hassane F, Saleh AF, Abes R, Gait MJ, Lebleu B. Cell penetrating peptides: overview and applications to the delivery of oligonucleotides. Cell Mol Life Sci 2010;67(5):715–26.
[20] Meade BR, Dowdy SF. Exogenous siRNA delivery using peptide transduction domains/cell penetrating peptides. Adv Drug Deliv Rev 2007;59(2–3):134–40.
[21] Torchilin VP, Rammohan R, Weissig V, Levchenko TS. TAT peptide on the surface of liposomes affords their efficient intracellular delivery even at low temperature and in the presence of metabolic inhibitors. Proc Natl Acad Sci USA 2001;98(15):8786–91.
[22] Torchilin VP. Cell penetrating peptide-modified pharmaceutical nanocarriers for intracellular drug and gene delivery. Biopolymers 2008;90(5):604–10.
[23] Vivès E, Richard JP, Rispal C, Lebleu B. TAT peptide internalization: seeking the mechanism of entry. Curr Protein Pept Sci 2003;4(2):125–32.
[24] Kaplan IM, Wadia JS, Dowdy SF. Cationic TAT peptide transduction domain enters cells by macropinocytosis. J Control Release 2005;102(1):247–53.
[25] Lee ES, Gao Z, Kim D, Park K, Kwon IC, Bae YH. Super pH-sensitive multifunctional polymeric micelle for tumor pH(e) specific TAT exposure and multidrug resistance. J Control Release 2008;129(3):228–36.
[26] Huang Y, Chen XM, Zhao BX, Ke XY, Zhao BJ, Zhao X, et al. Antiangiogenic activity of sterically stabilized liposomes containing paclitaxel (SSL-PTX): in vitro and in vivo. AAPS PharmSciTech 2010;11(2):752–9.
[27] Zhao BJ, Ke XY, Huang Y, Chen XM, Zhao X, Zhao BX, et al. The antiangiogenic efficacy of NGR-modified PEG-DSPE micelles containing paclitaxel (NGR-M-PTX) for the treatment of glioma in rats. J Drug Target 2011;19(5):382–90.
[28] Liu XR, Wu KC, Huang Y, Sun JB, Ke XY, Wang JC, et al. In vitro and in vivo studies on plasma-to-blood ratio of paclitaxel in human, rabbit and rat blood fractions. Biol Pharm Bull 2008;31(6):1215–20.
[29] Futaki S, Nakase I, Suzuki T, Youjun Z, Sugiura Y. Translocation of branched-chain arginine peptides through cell membranes: flexibility in the spatial disposition of positive charges in membrane-permeable peptides. Biochemistry 2002;41(25):7925–30.
[30] Lee ES, Shin HJ, Na K, Bae YH. Poly(L-histidine)-PEG block copolymer micelles and pH-induced destabilization. J Control Release 2003;90(3):363–74.
[31] Lee ES, Na K, Bae YH. Polymeric micelle for tumor pH and folate-mediated targeting. J Control Release 2003;91(1–2):103–13.
[32] Lee ES, Na K, Bae YH. Super pH-sensitive multifunctional polymeric micelle. Nano Lett 2005;5(2):325–9.
[33] Kim GM, Bae YH, Jo WH. pH-induced micelle formation of poly(histidine-co-phenylalanine)-block-poly(ethylene glycol) in aqueous media. Macromol Biosci 2005;5(11):1118–24.
[34] Gao ZG, Lee DH, Kim DI, Bae YH. Doxorubicin loaded pH-sensitive micelle targeting acidic extracellular pH of human ovarian A2780 tumor in mice. J Drug Target 2005;13(7):391–7.
[35] Futaki S, Ishikawa T, Niwa M, Kitagawa K, Yagami T. Embodying a stable alpha-helical protein structure through efficient chemical ligation via thioether formation. Bioorg Med Chem 1997;5(9):1883–91.
[36] Pan JG, Mak TW. Metabolic targeting as an anticancer strategy: dawn of a new era? Sci STKE 2007;2007(381):pe14.
[37] Leeper DB, Engin K, Thistlethwaite AJ, Hitchon HD, Dover JD, Li DJ. Human tumor extracellular pH as a function of blood glucose concentration. Int J Radiat Oncol Biol Phys 1994;28(4):935–43.
[38] Volk T, Jähde E, Fortmeyer HP, Glüsenkamp KH, Rajewsky MF. pH in human tumour xenografts: effect of intravenous administration of glucose. Br J Cancer 1993;68(3):492–500.
[39] Abdelrahim M, Konduri S, Basha R, Philip PA, Baker CH. Angiogenesis: an update and potential drug approaches (review). Int J Oncol 2010;36(1):5–18.
[40] Tozer GM, Kanthou C, Baguley BC. Disrupting tumour blood vessels. Nat Rev Cancer 2005;5(6):423–35.
[41] Neri D, Bicknell R. Tumour vascular targeting. Nat Rev Cancer 2005;5(6): 436–46.
[42] Jain RK. Normalization of tumor vasculature: an emerging concept in anti-angiogenic therapy. Science 2005;307(5706):58–62.
[43] Bode C, Trojan L, Weiss C, Kraenzlin B, Michaelis U, Teifel M, et al. Paclitaxel encapsulated in cationic liposomes: a new option for neovascular targeting for the treatment of prostate cancer. Oncol Rep 2009;22(2):321–6.
[44] Abu-Lila A, Suzuki T, Doi Y, Ishida T, Kiwada H. Oxaliplatin targeting to angiogenic vessels by PEGylated cationic liposomes suppresses the angiogenesis in a dorsal air sac mouse model. J Control Release 2009;134(1): 18–25.
[45] Ran S, Downes A, Thorpe PE. Increased exposure of anionic phospholipids on the surface of tumor blood vessels. Cancer Res 2002;62(21):6132–40.
[46] Makovitzki A, Fink A, Shai Y. Suppression of human solid tumor growth in mice by intratumor and systemic inoculation of histidine-rich and pH-dependent host defense-like lytic peptides. Cancer Res 2009;69(8): 3458–63.
[47] von Ardenne M. Principles and 1977 concept of cancer multistep therapy. Physiological fundamentals of the new timing. Selectotherm local hyperthermy. Arch Geschwulstforsch 1978;48(6):504–20.
[48] Lee ES, Na K, Bae YH. Doxorubicin loaded pH-sensitive polymeric micelles for reversal of resistant MCF-7 tumor. J Control Release 2005;103(2): 405–18.
[49] Gillies ER, Fréchet JM. pH-Responsive copolymer assemblies for controlled release of doxorubicin. Bioconjug Chem 2005;16(2):361–8.
[50] Drummond DC, Zignani M, Leroux J. Current status of pH-sensitive liposomes in drug delivery. Prog Lipid Res 2000;39(5):409–60.
[51] Lynn DM, Amiji MM, Langer R. pH-responsive polymer microspheres: rapid release of encapsulated material within the range of intracellular pH. Angew Chem Int Ed Engl 2001;40(9):1707–10.